Journal of Materials Chemistry C

Accepted Manuscript

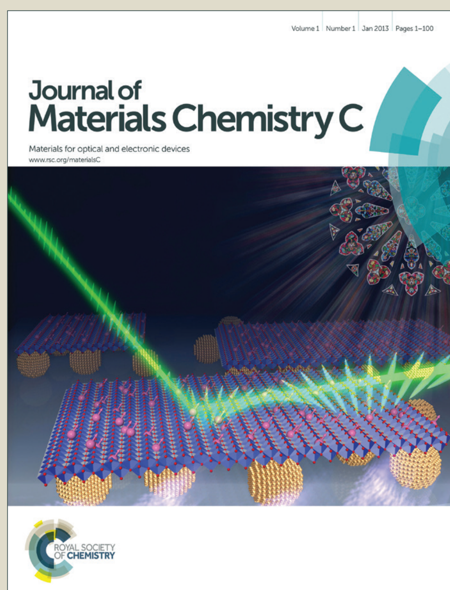

This is an *Accepted Manuscript*, which has been through the Royal Society of Chemistry peer review process and has been accepted for publication.

Accepted Manuscripts are published online shortly after acceptance, before technical editing, formatting and proof reading. Using this free service, authors can make their results available to the community, in citable form, before we publish the edited article. We will replace this *Accepted Manuscript* with the edited and formatted *Advance Article* as soon as it is available.

You can find more information about *Accepted Manuscripts* in the Information for Authors.

Please note that technical editing may introduce minor changes to the text and/or graphics, which may alter content. The journal's standard Terms & Conditions and the Ethical guidelines still apply. In no event shall the Royal Society of Chemistry be held responsible for any errors or omissions in this *Accepted Manuscript* or any consequences arising from the use of any information it contains.

ROYAL SOCIETY OF CHEMISTRY

www.rsc.org/materialsC

Dynamic Article Links ►

Cite this: DOI: 10.1039/c0xx00000x

www.rsc.org/xxxxxx

ARTICLE TYPE

Colossal Dielectric Constant of Amorphous TiO_2:(Nb, In) Film with Low Loss Fabricated at Room Temperature

Zhigang Gai[a,b], Zhenxiang Cheng*[a], Xiaolin Wang[a], Lanling Zhao[a], Na Yin[b], Roza Abah[b], Minglei Zhao[b], Fang Hong[a], Zheyin Yu[a] and Shixue Dou[a]

Received (in XXX, XXX) Xth XXXXXXXXX 20XX, Accepted Xth XXXXXXXXX 20XX

DOI: 10.1039/b000000x

The high-performance dielectric materials continue to arouse considerable interest due to the application in the field of solid state capacitor. In, Nb co-doped TiO_2 thin films with the composition of $(In_{0.5}Nb_{0.5})_xTi_{1-x}O_2$ (x= 0.10) was fabricated on Pt substrate by pulsed laser ablation at room temperature. In addition to their colossal permittivity ($\varepsilon_r > 4000$), they exhibit correspondingly low dielectric loss (about 5.5%) and high frequency-stability (up to 10 MHz), making the film suitable for myriad device miniaturization and high-energy-density storage applications. The preparation of this amorphous CP TiO_2 film at room temperature possesses great significance in microelectronic packaging not only because the CP film can be prepared on any kind of substrate even plastic or paper but also because the low temperature can protect the preparation of microelectronics devices. The procedure without annealing is simple and easy operation, which will raise the efficiency and reduce the production cost in semiconductor industry. As remarked above, In, Nb co-doped amorphous TiO_2 films with colossal permittivity would be a highly attractive proposition.

Introduction

In recent years, due to the globle warming effect and the urgent need for clean and renewable energy, not only energy harvesting, but also energy storage have become key issues for fullfilling this need. High-performance dielectric materials have been attracting increasing attention because of their applications in myriad types of miniaturized devices and in high-energy-density storage applications. [1,2] With the trend towards size reduction of many microelectronic devices, high-dielectric-constant oxides have become essential for modern microelectronics devices, such as dynamic random access memory (DRAM) devices and on-chip capacitors. Another important aspect for device fabrication and integration is low processing temperature, which can not only reduce energy consumption during fabrication, but also can improve material processing compatibility (without degrading other parts of the device).

The colossal permittivity (CP) materials, such as doped $BaTiO_3$ perovskites, [3] $CaCu_3Ti_4O_{12}$ (CCTO), [4,5] doped NiO, $La_{2x}Sr_xNiO_4$, [6,7] etc. have been fully accepted as excellent materials for such purposes due to their prodigiously high, temperature-independent permittivity. In addition to the broad structural range of these materials, extensive research has been carried out in to investigate acceptor and donor dopants to further enhance their dielectric properties. [8,9]

The high permittivity of the doped $BaTiO_3$ perovskites can only be achieved over a narrow temperature range close to the ferroelectric phase transition (at ~120°C). The dielectric losses of non-ferroelectric materials showing colossal values of ε such as $CaCu_3Ti_4O_{12}$ (CCTO), doped NiO, and $La_{2x}Sr_xNiO_4$, are relatively high (over 10%), which makes real applications for them impossible due to their huge energy dissipation during operation. [3,5,10-14] An effective strategy to achieve an appropriate balance between having a stable CP and achieving an affordable low dielectric loss for practical applications is still lacking, because most of the approaches employed to improve one dielectric parameter always degrade the other.[15] The difficulty in achieving both CP and low dielectric loss in a single material has greatly impeded the practical application of CP materials.[16,17]

To further enhance dielectric permittivity, but with acceptable dielectric loss and less frequency/temperature dependence, the introduction of localized lattice defect states was proposed very recently in work published in Nature Materials. [18-22] The TiO_2 material system chosen in this study shows a high dielectric permittivity greater than 10,000 with a with dielectric loss about 5%. Given its abundance and low toxicity, doped TiO_2 materials with colossal permittivity would be a highly attractive proposition. It was noticed the reported giant dielectric constant was realized in doped rutile phase of TiO_2, which usually needs high temperature for phase formation. Such high temperate processing is not favourable to the integration of electronic devices. In addition, the introduction of codoping of Nb and In will form localized lattice defect states in crystalline TiO_2, which is a key for displaying giant dielectric constant and loss loss. Whether such localized lattice defect states can still form in short range ordered non-crystalline material is an open question, which will favour to the designation similar material systems with gigant dielectric constant. Therefore further exploration of the doped TiO_2 in terms of the impact of the fabrication condition and the crystallinity on the dielectric properties is of practical importance. In this work, $(In_{0.5}Nb_{0.5})_xTi_{1-x}O_2$ (x = 0.00, 0.10) films were prepared using the pulsed laser deposition (PLD) method at room temperature, and the dielectric properties were investigated. The best dielectric properties reported in the literature were for the x = 0.10 composition,[22] and therefore, this

Journal of Materials Chemistry C Accepted Manuscript

specific composition was selected for making the thin film. Results show that doped TiO_2 thin film in an amorphous form with large dielectric constant up to a few thousand and low loss were obtained at room temperature.

Experimental

The starting materials used for the fabrication of the target were high purity rutile TiO_2 (99.99%, Aldrich), Nb_2O_5 (99.99%, Stanford Materials), and In_2O_3 (99.99%, Aldrich),. The materials were weighed out according to the composition $(In_{0.5}Nb_{0.5})_xTi_{1-x}O_2$, with some excess In_2O_3 used to compensate for the loss of volatile In_2O_3 at high temperature, and then mixed using ball milling, dried, and calcined at 900°C for 2 h. After calcination, the ball-milled ground powders were pressed into disks 20 mm in diameter and 4 mm in thickness. Densification was achieved by sintering the disks at 1400°C for 5–10 h in a sealed crucible to prevent volatilization.

The excimer laser used for PLD is the third harmonic generation of a Nd:YAG (yttrium aluminum garnet) laser with a wavelength of 355 nm and intensity of 2–3 J cm^{-2} at a repetition rate of 10 Hz. The distance between the target and the substrate was 35 mm. The deposition was in 1 mTorr dynamic oxygen at room temperature. An upper electrode with dimensions of 0.0314 mm^2 was covered with a shadow mask and coated by magnetron sputtering. The dielectric behavior of the $Pt/TiO_2/Pt$ capacitor was measured using an Impedance Analyzer (Agilent 4294A) from 40 to 10 MHz as a function of frequency. The crystal structure of the films was examined by X-ray diffraction (XRD, Model: GBC MMA), using Cu K_α radiation at λ = 1.54056 Å from 20° to 80°. Characterization of the microstructure of the films was conducted by scanning electron microscopy (SEM, JEOL JDX-3500). The thickness of the grown film which was measured by observation of the cross-section of the film using SEM, is typically 550 nm. The oxidation states of Ti and oxygen were determined by XPS. A saturated structured illumination microscope (SSIM) probe XPS was used, employing an Al $K\alpha$ (hν = 1486.6 eV) excitation source. High resolution XPS spectra were collected at 26 eV pass energy with a dwell time of 100 ms per point. Peak positions were referenced to the C 1s peak at 284.8 eV. The binding energies of the Ti 2p and O 1s peaks were examined.

Results and discussion

Figure 1 shows a high resolution X-ray diffraction (XRD) scan (2θ = 20° to 80°) of the prepared TiO_2 thin films deposited at room temperature. The X ray diffraction pattern of the Pt/Si substrate was also plotted for reference purposes [Figure 1(a)]. Because of the Pt substrate attached to the Si surface and the Si natural oxidation, the XRD pattern of the Pt/Si substrate contains diffraction peaks from Pt, Si, and SiO_2 in the range from 20° to 80°. Figure 1(b) and (c) presents XRD patterns of the TiO_2 and TiO_2:(In,Nb) films prepared on Pt/Si substrate, respectively. Besides the diffraction peaks from the Pt/Si substrate, no peaks corresponding to TiO_2 rutile phase or anatase phase was successfully detected in Figure 1(b) and (c). Moreover, the X-ray diffraction patterns of In_2O_3 and Nb_2O_5 are not found in the XRD reflections of the films, which indicates that In^{3+} and Nb^{5+} were doped into the Ti^{4+} sites instead of forming impurities. It has been reported that TiO_2 is amorphous when the growth temperature is under 300℃.[23] The lack of any detectable diffraction peak in the range of 2θ = 20° to 80° from our In, Nb doped and undoped TiO_2 films shows that amorphous phase was obtained. Figure 1(d) and (e) contains the X-ray diffraction spectra of the rutile phase and the anatase phase of pure TiO_2, respectively, placed here for comparison.

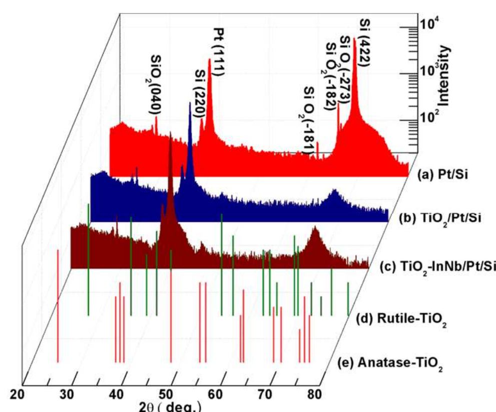

Fig.1 XRD patterns of amorphous TiO_2 films: (a) Pt/Si substrate, (b) pure TiO_2 film prepared on the Pt/Si substrate, (c) TiO_2-(In, Nb) film prepared on the Pt/Si substrate, (d) pure rutile TiO_2, (e) pure anatase TiO_2.

Figure 2 presents a scanning electron microscope (SEM) micrograph of the surface of the TiO_2:(In,Nb) film obtained by PLD. Although the uniform surface of the film shows some inhomogeneity, no observable nano-sized particles could be found, even at a very high resolution (×200,000). The failure to observe such particles and particle grain boundaries strongly suggests that the films are in the amorphous state. The crystallization of doped and undoped TiO_2 was seriously hindered by the low processing temperature (room temperature).

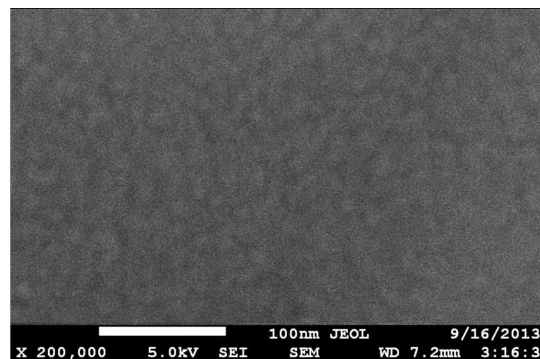

Fig.2 SEM micrograph of the surface of the TiO_2-(In, Nb) film.

The Raman spectra of the TiO_2-based films and the spectra of pure rutile and anatase TiO_2 are presented in Figure 3. The Raman spectra of the doped and undoped TiO_2 thin films prepared by PLD at room temperature do not show any clear

This journal is © The Royal Society of Chemistry [year]
Journal of Materials Chemistry C Accepted Manuscript

characteristic spectral peaks, such as are observed for the standard samples of pure rutile and anatase TiO_2 shown in Fig. 3, except for two large bumps, which indicates the amorphous state. One wide bump approximately covers the zone from 143 cm^{-1}, which is assigned to the corresponding B_{1g} mode of rutile (superimposed with the 144 cm^{-1} band corresponding to the E_g mode of anatase), to 197 cm^{-1}, which is assigned to the corresponding E_g mode of anatase. The other bump can be found within the zone from 609 cm^{-1} (which is assigned to the corresponding A_{1g} mode of rutile phase) to 640 cm^{-1} (the E_g mode of rutile). That these two broad bumps are spread over the wavenumber zones covering some typical vibration peaks from both anatase and rutile phases in the very sensitive Raman spectra proves that the TiO_2 in the two films is amorphous. All in all, the TiO_2 in the two films does not have any long-range order, as is evident from the absence of any clear vibration peaks corresponding to pure rutile or anatase TiO_2, which further proves that the TiO_2 film fabricated at room temperature in this work is amorphous.

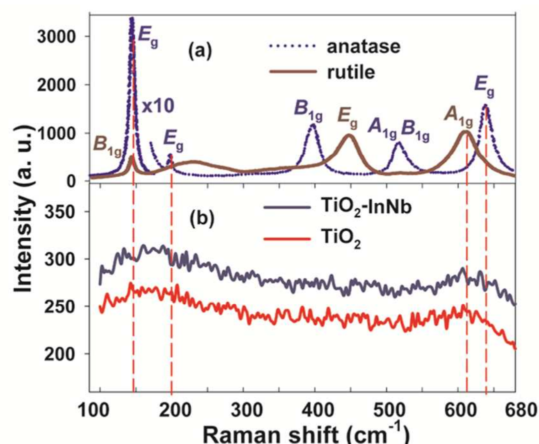

Fig.3 Raman spectra of TiO_2-based films: (a) Raman spectra of anatase TiO_2 and rutile TiO_2; (b) Raman spectra of the undoped TiO_2 film and the (In, Nb) dopedTiO_2- film

Figure 4 shows the relative dielectric permittivity ($\varepsilon/\varepsilon_0$) and dielectric loss (tanδ) measured at room temperature as a function of frequency for the doped and undoped TiO_2 films. As expected, the dielectric permittivity of the pure amorphous TiO_2 film in this work was found to be 195，which is slightly higher than for other phases of crystallized TiO_2 (where the dielectric permittivity ($\varepsilon/\varepsilon_0$) was reported to be 170).[24] The dielectric permittivity of the (In, Nb) co-doped amorphous TiO_2 is improved greatly by more than an order of magnitude. At 1 MHz, the dielectric permittivity is enhanced from 195 to 3983, by more than 20 times. In addition, the dielectric permittivity is always higher than 4000 in the wide range from 100 Hz to 0.9 MHz. The dielectric permittivity decreases slowly with increasing frequency, but it is still above 3070 at the very high frequencies up to 10 MHz. At the same time, the dielectric loss of the (In, Nb) co-doped amorphous TiO_2 thin film is reduced significantly. At 1 MHz, the dielectric loss is decreased from 32% to 6%, which is more than a 5-fold reduction. Over the whole frequency range, the dielectric loss of the doped TiO_2 decreases relatively quickly from the starting frequency to 663 kHz, where its value is 5.8%, and then it increases slowly until 4.9 MHz, where it begins to decrease slowly from the loss peak value of 10.0%. Up to the end of the frequency range, 10 MHz, the loss decreases to 5.5%. Over a broad frequency range from 75 kHz to 10 MHz, the dielectric loss is less than 10.0%. The frequency dependence of the dielectric behavior in the range of 100 Hz – 10 MHz was found to be very low, demonstrating that the dielectric properties of the (In, Nb) co-doped amorphous TiO_2 films possess very high frequency stability.

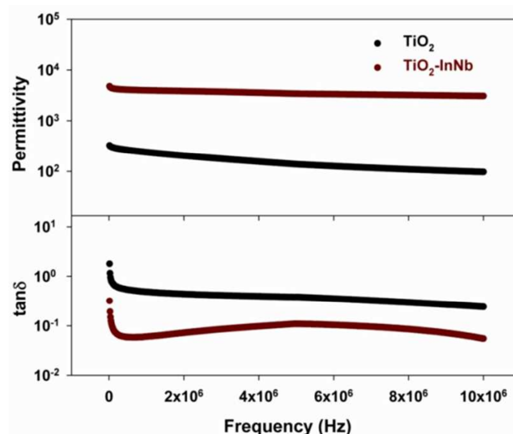

Fig.4 Frequency dependence of the dielectric properties of the (In, Nb) co-doped amorphous TiO_2 film fabricated at room temperature.

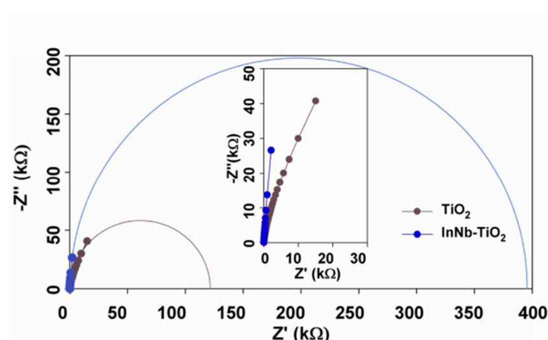

Fig.5 Complex impedance plots [Z′(ω)-Z″(ω)] of pure TiO_2 and 10% (In, Nb) co-doped TiO_2 films measured at room temperature, and corresponding fitting results (solid lines) using a Cole–Cole model. The inset is an enlargement of the indicated range.

Figure 5 shows the complex electrochemical impedance spectrum of the 10% (In, Nb) co-doped TiO_2 film, where the solid lines correspond to the fitting results using a Cole-Cole model, and a plot of the complex impedance of the un-doped TiO_2 film is also given for comparison purposes. As can be clearly seen from Figure 5, the Cole-Cole semicircle size of the (In, Nb) co-doped TiO_2 film is apparently about 3 times greater than that of the un-doped TiO_2 film, demonstrating the sharp increase in the resistivity caused by the co-doping with (In, Nb). The changes in the electric field inside the molecules caused by the (In, Nb) doping block the movement of electrons, finally resulting in increased resistivity. Only an essentially linear arc

Journal of Materials Chemistry C Accepted Manuscript

with a high-frequency near-zero intercept is observed for each complex impedance plot (as is more clearly seen from the enlarged figure in the inset of Fig. 5) measured at room temperature. This means that the complex impedance contains only one constituent contribution at the atomic level, which can be considered to be the source of the colossal dielectric permittivity, while it has nothing to do with any grain boundary effect.[25] The results are also in consonance with the amorphous phase TiO_2 without apparent grain boundaries and long-range order as discussed earlier.

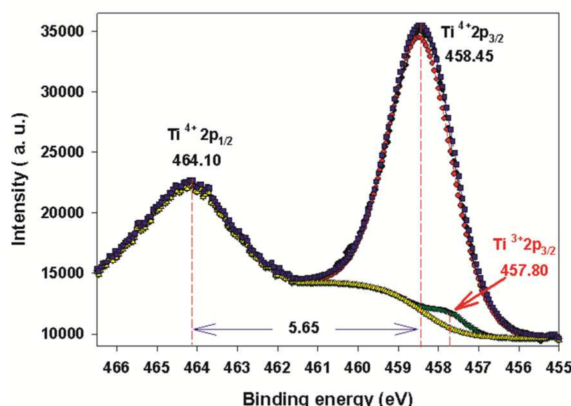

Fig.6 Ti 2p spectrum of the (In, Nb) co-doped amorphous TiO_2 film at room temperature.

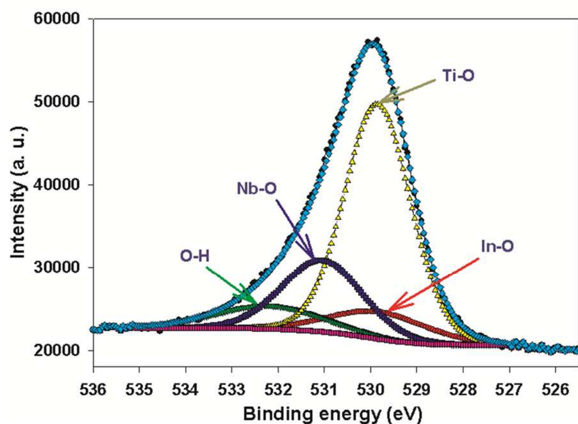

Fig.7 O 1s spectrum of the (In, Nb) co-doped amorphous TiO_2 film at room temperature.

The chemical states and chemical compositions of the samples were investigated through X-ray photoelectron spectroscopy (XPS). Fig. 6 shows the Ti 2p XPS spectrum of the as-prepared sample. The XPS results indicate that the binding energies of the Ti 2p doublet with $2p_{3/2}$ and $2p_{1/2}$ are 458.45 eV and 464.10 eV, respectively, which are in good agreement with the literature values. [26,27] The separation of the Ti $2p_{3/2}$ and Ti $2p_{1/2}$ peaks (the spin-orbit splitting) is 5.65 eV, indicating that titanium mainly exists as Ti^{4+}. In addition, the desummation of the spectrum results in a small peak belonging to Ti^{3+}, for which the Ti $2p_{3/2}$ peak is located at about 457.80 eV.[28] The noticeable Ti^{3+} signal gives a Ti^{3+}/Ti^{4+} proportion of 3.27% for the 10% (In, Nb) co-doped sample. This gives a Ti^{3+} content of 2.85%, less than the initially introduced individual dopant amounts (5% each for Nb and In). The introduction of Nb^{5+} into the TiO_2 must be an important reason for the appearance of the low valence Ti^{3+} ions. Meanwhile, the presence of In^{3+} can help the Ti^{4+} to maintain its valence of +4.[26] The reaction equations of the partial reduction of Ti^{4+} to Ti^{3+} are as follows:

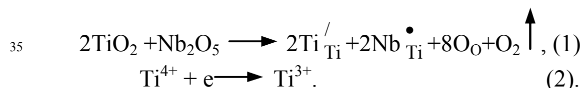

$$2TiO_2 + Nb_2O_5 \longrightarrow 2Ti'_{Ti} + 2Nb^{\bullet}_{Ti} + 8O_O + O_2\uparrow, \quad (1)$$

$$Ti^{4+} + e \longrightarrow Ti^{3+}. \quad (2).$$

The Nb^{5+} substituting for Ti^{4+} with an added positive charge turns one of the surrounding Ti^{4+} ions into Ti^{3+} through obtaining a negative electron because of the demand for charge balance, but the In^{3+} substituting for Ti^{4+} with a lesser positive charge needs a corresponding positive charge to come into being around the surrounding Ti^{4+} to balance the charges, which can make the Ti^{4+} keep its highest valence of +4. Since the In element is violate during fabrication process, the final composition of the fabricated amorphous film is determined by the overall X-ray photoelectron spectroscopy: 3.65 % In^{3+}, 5.07 % Nb^{5+}, 91.28% Ti (include about 2.85% Ti^{3+} as noted earlier). The total amount of In^{3+} (3.65 %) and Ti^{3+} (2.85%) is a little more than Nb^{5+} (5.07 %), which will cause the presence of some oxygen vacancies due to the need to maintain charge balance.

As shown in Fig. 7, the O 1s XPS spectrum of the co-doped TiO_2 consists of a broad asymmetric peak, which can be fitted with four peaks. The strongest peak at 529.85 eV corresponds to bulk oxygen bonded to titanium. The two higher-energy peaks corresponding to the bulk In-O and Nb-O cation-oxygen bonds are at 530.05 eV and 531.10 eV, respectively. The highest-energy peak at 532.30 eV is assigned to adsorbed surface H_2O, as well as the presence of surface hydroxyl groups and oxygen vacancies.[29] It is well known that In^{3+} doped into TiO_2 as an acceptor requires oxygen vacancies for charge compensation.[27] The reaction equations are as follows:

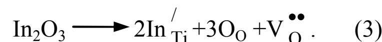

$$In_2O_3 \longrightarrow 2In'_{Ti} + 3O_O + V^{\bullet\bullet}_O. \quad (3)$$

As mentioned above, Ti^{4+}, In^{3+}, Nb^{5+}, Ti^{3+} (produced by the Nb^{5+}), and oxygen vacancies (caused by In^{3+}) all coexist in the In, Nb co-doped TiO_2 film, acting together to maintain the balance of charges. As a result, the oxygen vacancy, $V^{\bullet\bullet}_O$, with two positive charges can be connected with the nearest In^{3+} and Ti^{3+} (Ti^{4+} + e), respectively, with one less negative charge to form the correlated electric dipole:

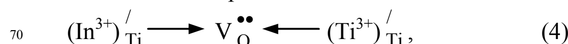

$$(In^{3+})'_{Ti} \longrightarrow V^{\bullet\bullet}_O \longleftarrow (Ti^{3+})'_{Ti}, \quad (4)$$

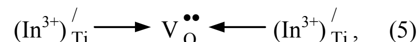

$$(In^{3+})'_{Ti} \longrightarrow V^{\bullet\bullet}_O \longleftarrow (In^{3+})'_{Ti}, \quad (5)$$

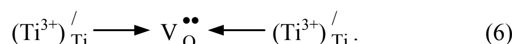

$$(Ti^{3+})'_{Ti} \longrightarrow V^{\bullet\bullet}_O \longleftarrow (Ti^{3+})'_{Ti}. \quad (6)$$

Meanwhile, the $Nb^{\bullet}_{Ti}$ (Nb^{5+}) with one positive charge can also form electric dipoles as shown below:

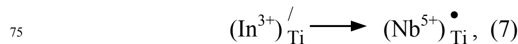

$$(In^{3+})'_{Ti} \longrightarrow (Nb^{5+})^{\bullet}_{Ti}, \quad (7)$$

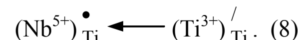

$$(Nb^{5+})^{\bullet}_{Ti} \longleftarrow (Ti^{3+})'_{Ti}. \quad (8)$$

Under these circumstances, the $V^{\bullet\bullet}_O$ and $Nb^{\bullet}_{Ti}$ with positive charges can all unite with the $(In^{3+})'_{Ti}$ and $(Ti^{3+})'_{Ti}$ with positive

Journal of Materials Chemistry C Accepted Manuscript

This journal is © The Royal Society of Chemistry [year]

charges to form complex electric dipoles which are correlated and overlap each other. These electric defect-dipole clusters do not exist independently; they influence and become involved with each other. The additional bound electrons are highly localized in the zones of these electric dipoles and tightly bound by the local defect clusters, such as $(In^{3+})^{/}_{Ti} \longrightarrow V^{\bullet\bullet}_{O}$, $2(In^{3+})^{/}_{Ti} \longrightarrow V^{\bullet\bullet}_{O} + (Nb^{\bullet}_{Ti})$, $V^{\bullet\bullet}_{O} \longleftarrow (Ti^{3+})^{/}_{Ti}$, $(Nb^{\bullet}_{Ti} + V^{\bullet\bullet}_{O}) \longleftarrow (In^{3+})^{/}_{Ti} + (Ti^{3+})^{/}_{Ti}$, $(2Nb^{\bullet}_{Ti} + V^{\bullet\bullet}_{O}) \longleftarrow 2(Ti^{3+})^{/}_{Ti}$, etc. The pinning effect on electrons of the electric defect-dipoles results in both high permittivity and low dielectric loss over a relatively wide frequency range, as experimentally observed. Remarkably, the (In, Nb) co-doped TiO_2 thin film is amorphous phase, which has no apparent grain boundaries, indirectly proving that this pinning effect on electrons of the electric defect-dipoles exists in the short range at the atomic level, while it has nothing to do with any grain boundary effect. For the Internal Barrier Layer Capacitance, the electrons range over a large distance in the grain, being hindered by the grain boundary, which causes the electron responses are mainly at low frequency, and the dielectric losses are extra large at high frequency. However, the electrons tightly bound by the local electric dipole defect clusters in the (In, Nb) co-doped TiO_2 amorphous film can only range over a very small distance because of being trapped in the small zones around these defect clusters. These electric defect-dipoles of huge amounts are homogenously distributed throughout the material, which leads to a response to external electrical field in a more broad frequency range while maintaining a low dielectric loss. For such a case, the Maxwell-Wagner effect due to space charge trapped at dipole defect centers will dominate the large dielectric constant.[30] Therefore, our (In, Nb) co-doped amorphous TiO_2 thin films obtained at room temperature display both high permittivity and low dielectric loss over a wide frequency range.

Conclusions

In summary, (In, Nb) co-doped amorphous TiO_2 thin films were fabricated by PLD at room temperature. (In, Nb) modification of TiO_2-based materials resulted in obvious improvement of the dielectric properties. The dielectric permittivity of the (In, Nb) co-doped amorphous TiO_2 was improved greatly by more than one order of magnitude, reaching a value of more than 4000. Meanwhile, the dielectric loss of the doped amorphous TiO_2 is reduced significantly, by more than 5 times, to a minimum of 5.5%. The dielectric properties of the amorphous TiO_2-based film exhibit very stable frequency behavior, and this, together with its colossal permitivity and very low dielectric loss, makes the (In, Nb) modified TiO_2-based film a promising candidate for semiconductor industry applications. The preparation of this amorphous CP TiO_2 film at room temperature has great significance for microelectronic packaging, not only because the CP film can be prepared on any kind of substrate, even plastic or paper, but also because its suitability for low temperature preparation can avoid damage to microelectronic devices. The procedure, which requires no annealing, is simple and easy, which will raise efficiency and reduce production costs in the semiconductor industry. As remarked above, doped TiO_2 films with colossal permittivity would be a highly attractive proposition. In addition, the physical mechanism of the electron-pinning effect of the electric defect-dipoles resulting in perfect dielectric behavior in crystalline rutile TiO_2 still works in short range order amorphous phase, which will arouse interest in investigating the details and applying it to other materials.

Z. X. Cheng thanks the Australian Research Council for support. All the authors thank Dr. Tania Silver for carefully polishing the paper. This work is also supported by the National Natural Science Foundation of China (51002087, 51172129) and the Natural Science Foundation of Shandong Province (ZR2013EMM018, ZR2013EMM014).

Notes and references

[a] *Institute for Superconducting and Electronic Materials, University of Wollongong, North Wollongong, NSW 2500, Australia. Fax: 61-2-42215731; Tel: 61-2-42981406; E-mail: cheng@uow.edu.au*
[b] *School of Physics, State Key Laboratory of Crystal Materials, Shandong University, Jinan 250100, P. R. China. Fax: 86-531-88377098; Tel: 86-531-88365997; E-mail: gzg@sdu.edu.cn*

† Electronic Supplementary Information (ESI) available: [details of any supplementary information available should be included here]. See DOI: 10.1039/b000000x/

‡ Footnotes should appear here. These might include comments relevant to but not central to the matter under discussion, limited experimental and spectral data, and crystallographic data.

1 C. C. Homes, T. Vogt, S. M. Shapiro, S. Wakimoto, A. P. Ramirez, *Science* , 2001, **293**, 673;
2 S. Krohns, P. Lunkenheimer, S. Meissner, A. Reller, B. Gleich, A.Rathgeber, T. Gaugler, H. U. Buhl, D. C. Sinclair, A. Loidl, *Nature Mater.* , 2011, **10**, 899;
3 M. T. Buscaglia, M. Viviani, V. Buscaglia, L. Mitoseriu, A. Testino, P. Nanni, Z. Zhao, M. Nygren, C. Harnagea, D. Piazza, C. Galassi, *Phys. Rev. B* ,2006, **73**, 064114;
4 M. A.Subramanian, D. Li, N. Duan, B. A. Reisner, A.W. Sleight, *J. Solid State Chem.*, 2000, **151**, 323;
5 A.P. Ramirez, M. A. Subramanian, M. Gardel, G. Blumberg, D. Li, T. Vogt, S. M. Shapiro, *Solid State Commun.*, 2000, **115**, 217;
6 J. B.Wu, C. W. Nan, Y. H. Lin, Y. Deng, *Phys. Rev. Lett.* , 2002, **89**, 217601;
7 S.Krohns, P.Lunkenheimer, Ch. Kant, A. V. Pronin, H. B. Brom, A. A. Nugroho, M. Diantoro, A. Loidl, *Appl. Phys. Lett*., 2009, **94**, 122903;
8 N.Ikeda, H. Ohsumi, K. Ohwada, K. Ishii, T. Inami, K. Kakurai, Y. Murakami, K. Yoshii, S. Mori, Y. Horibe, H. Kitô, *Nature*, 2005, **436**, 1136;
9 C. C.Wang, L. W. Zhang, *Appl. Phys. Lett*., 2006, **88**, 042906;
10 M. Li, A. Feteira, D. C. Sinclair, A. R. West, *Appl. Phys. Lett*., 2006, **88**, 232903;
11 Y. Liu, R. L. Withers, X. Y. Wei, *Phys. Rev. B* , 2005, **72**,134104;
12 Y.Zhu, J. C. Zheng, L. Wu, A. I. Frenkel, J. Hanson, P. Northrup, W. Ku, *Phys. Rev. Lett.*, 2007, **99**, 037602;
13 L. Zhang, Z. J. Tang, *Phys. Rev. B* , 2004, **70**, 174306;
14 S. Krohns, P. Lunkenheimer, S. G. Ebbinghaus, A. Loidl, *J. Appl. Phys.* , 2008, **103**, 084107;
15 S. Guillemet-Fritsch, Z. Valdez-Nava, C. Tenailleau, T. Lebey, B. Durand, J. Y. Chane-Ching, *Adv. Mater.*, 2008, **20**, 551;
16 P. Lunkenheimer, V. Bobnar, A. V. Pronin, A. I. Ritus, A. A. Volkov, A. Loidl, *Phys. Rev. B*, 2002, **66**, 052105;
17 P.Lunkenheimer, S. Krohns, S. Riegg, S.G. Ebbinghaus, A. Reller, A. Loidl, *Eur. Phys. J.* , 2010, **180**, 61;
18 M. H. Whangbo, M. A. Subramanian, *Chem. Mater*., 2006, **18**, 3257;
19 M. Wuttig, N. Yamada, *Nature Mater.*, 2007, **6**, 122;
20 N.Balke, B. Winchester, W. Ren, Y. H. Chu, N. Anna Morozovska, E. A. Eliseev, M. Huijben, R. K. Vasudevan, P. Maksymovych, J.Britson, S. Jesse, I. Kornev, R. Ramesh, L. Bellaiche, L. Chen, S. V. Kalinin, *Nature Phys.*, 2012, **8**, 81.
21 J. C.Zheng, A. I. Frenkel, L. Wu, J. Hanson, W. Ku, E. S. Božin, S. J. Billinge, L. Y. Zhu, *Phys. Rev. B*, 2010, **81**, 1442.
22 W. Hu, Y. Liu, R. L. Withers, T. J. Frankcombe, L. Norén, A. Snashall, M. Kitchin, P. Smith, B. Gong, H. Chen, J. Schiemer, F. Brink, Wong-Leung, *Nature Mater*., 2013, **12**, 821.

Journal of Materials Chemistry C Accepted Manuscript

23 X. Xiao, W. Wang, S. Li, Y. Liu, D. Zhang, S. Qiang, X. Gao, B. Zhang, *Chinese J. Lasers*, 2013, **140**, 0207001.

24 L.Forro, O. Chauvet, D. Emin, L. Zuppiroli, H. Berger, F. Lévy, *J. Appl. Phys.*, 1994, **75**, 633.

25 J.Yang, J. He, J. Y. Zhu, W. Bai, L. Sun, X. J. Meng, X. D. Tang, C. G. Duan, D. Remiens, J. H. Qiu, J. H. Chu, *Appl. Phys. Lett.*, 2012, **101**, 222904.

26 I. Ganesh, A. K. Gupta, P. P. Kumar, P. S. Chandra Sekhar, K. Radha, G. Padmanabham, G. Sundararajan, *Mater. Chem. Phys.*, 2012, **135**, 220.

27 D. Morris, Y. Dou, J. Rebane, C. E. J. Mitchell, R. G. Egdell, *Phys. Rev. B*, 2000, **61**, 13445.

28 C.Trapalis, V. Kozhukharov, B. Samuneva, *J. Mater. Sci.*, 1993, **28**, 1276.

29 E. Ramos-Moore, P. Ferrari, D. E. Diaz-Droguett, D. Lederman, J. T. Evans, *J. Appl. Phys.*, 2012, **111**, 014108.

30 F.Hong, Z. Cheng, X. Wang, *J. Appl. Phys.*, 2012, **112**, 013920.

Journal of Materials Chemistry C Accepted Manuscript

 This journal is © The Royal Society of Chemistry [year]